Journal of Nuclear Materials 392 (2009) 379–385

Contents lists available at ScienceDirect

Journal of Nuclear Materials

journal homepage: www.elsevier.com/locate/jnucmat

Evaluation of alloy 690 process pot at the contact with borosilicate melt pool during vitrification of high-level nuclear waste

Pranesh Sengupta [a,*], C.P. Kaushik [b], G.B. Kale [a], D. Das [c], K. Raj [c], B.P. Sharma [d]

[a] Materials Science Division, Bhabha Atomic Research Centre, Mumbai 400 085, India
[b] Waste Management Division, Bhabha Atomic Research Centre, Mumbai 400 085, India
[c] Chemistry Division, Bhabha Atomic Research Centre, Mumbai 400 085, India
[d] Chemical Engineering Group, Bhabha Atomic Research Centre, Mumbai 400 085, India

ARTICLE INFO

Article history:
Received 9 April 2007
Accepted 24 July 2008

PACS:
81.65.kn
21.65.+f
81.05.kf

ABSTRACT

Understanding the material behaviour under service conditions is essential to enhance the life span of alloy 690 process pot used in vitrification of high-level nuclear waste. During vitrification process, interaction of alloy 690 with borosilicate melt takes place for substantial time period. Present experimental studies show that such interactions may result in Cr carbide precipitation along grain boundaries, Cr depletion in austenitic matrix and intergranular attack close to alloy 690/borosilicate melt pool interfaces. Widths of Cr depleted zone within alloy 690 is found to follow kinetics of the type $x = 10.9 \times 10^{-6} + 1 \times 10^{-8} t^{1/2}$ m. Based on the experimental results it is recommended that compositional modification of alloy 690 process pot adjacent to borosilicate melt pool need to be considered seriously for any efforts towards reduction and/or prevention of process pot failures.

1. Introduction

Failure of vitrification melter pots is considered as a serious issue in Waste Immobilization Plants (WIP) engaged in immobilization of high-level nuclear waste (HLW). Such failures not only interrupt HLW immobilization process, but also create huge task of decommissioning and disposing of failed melter pots. On the whole, these failures make vitrification process rather expensive. Thus, proper understanding of melter pot failure mechanism is necessary for smooth plant operations. One major handicap for such understandings is that the failed pots cannot be examined from close due to containment of radioactivity in it. Decontamination of the process pot is also not an easy task. Hence, in most of the cases the only direct data available from failed pot are the digital images taken by camera during plant operation and decommissioning. This leaves material scientists in a difficult situation as melter pot failures can be governed by many factors. Starting from design of the melter pot itself the reasons of failures can be anything from response of the parent materials and weldments to the thermal cycles, their interaction with HLW, molten waste glass, etc. Thus, for a clear understanding of melter pot failures, detailed documentation of materials' response to service condition is required. As a step towards this, a project has been undertaken to understand the failures of alloy 690 process pots used at WIP Trombay, Bhabha Atomic Research Centre. A brief note on the alloy 690 process pot is given below.

As shown in Fig. 1, the metallic melter pot design is based on multiple containment concept actual vitrification process takes place within alloy 690 process pot that is surrounded successively by susceptor (also made up of alloy 690) and thermal insulator. The process pot has three major parts namely, top dish, cylindrical cell and bottom dish. The cell is joined with top and bottom dishes by TIG welding. During operation, susceptor is heated by multizone induction furnace and it radiates heat to process pot to raise its temperature to desired value. Thermowell made of alloy 690 is attached to process pot to monitor the temperature of borosilicate melt pool and empty space above that. Operating temperature of process pot depends on the pouring temperature of the borosilicate melt and vitrification process flow chart. At WIP Trombay, sodium–barium borosilicate waste glass is being prepared to immobilize sulfate containing HLW [1,2]. The process is done in step-wise manner, which include mixing of HLW and glass forming slurry, evaporation, calcination, melt formation and soaking. It is during the soaking stage that significant interaction between process pot and borosilicate melt pool takes place. Since pouring temperature for sodium–barium borosilicate melt is close to 1173 K so to maintain this as centerline temperature the lower portion of process pot is generally kept at 1223 K.

Recent failures of process pots at WIP Trombay, made it necessary to remove them from plant facility. Before removal, the pots were visually inspected using remote digital camera systems. Records show that material failures have mostly taken place in the form of intergranular crack, pore etc, within the lower part of cell

* Corresponding author. Tel.: +91 22 2559 0468; fax: +91 22 2550 5239.
E-mail address: sengupta@barc.gov.in (P. Sengupta).

0022-3115/$ - see front matter © 2008 Elsevier B.V. All rights reserved.
doi:10.1016/j.jnucmat.2008.07.046

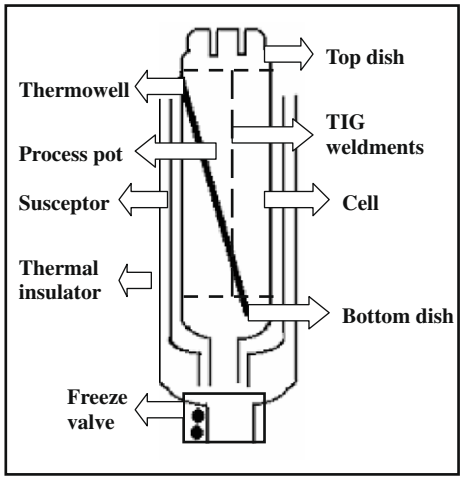

Fig. 1. Schematic diagram of induction metallic melter used at WIP, Trombay.

and bottom dish where borosilicate melt is being produced. These have developed on parent material as well as at or close to TIG welded zone. Similar failures have been observed within alloy

Table 1
Composition of alloy 690 used in melter pots

Element (wt%)	Alloy 690
Cr	27.00–31.00
Fe	7–11
Cu	0.50 Max
Si	0.50 Max
Mn	0.50 Max
S	0.01 Max
C	0.05 Max
Ni	Remaining
Melting range (°C)	1343–1377

Table 2
Composition of the borosilicate melt [2]

Component	Concentration (wt%)
SiO_2	30.5
B_2O_3	20
Na_2O	9.5
BaO	19
Waste oxides	21

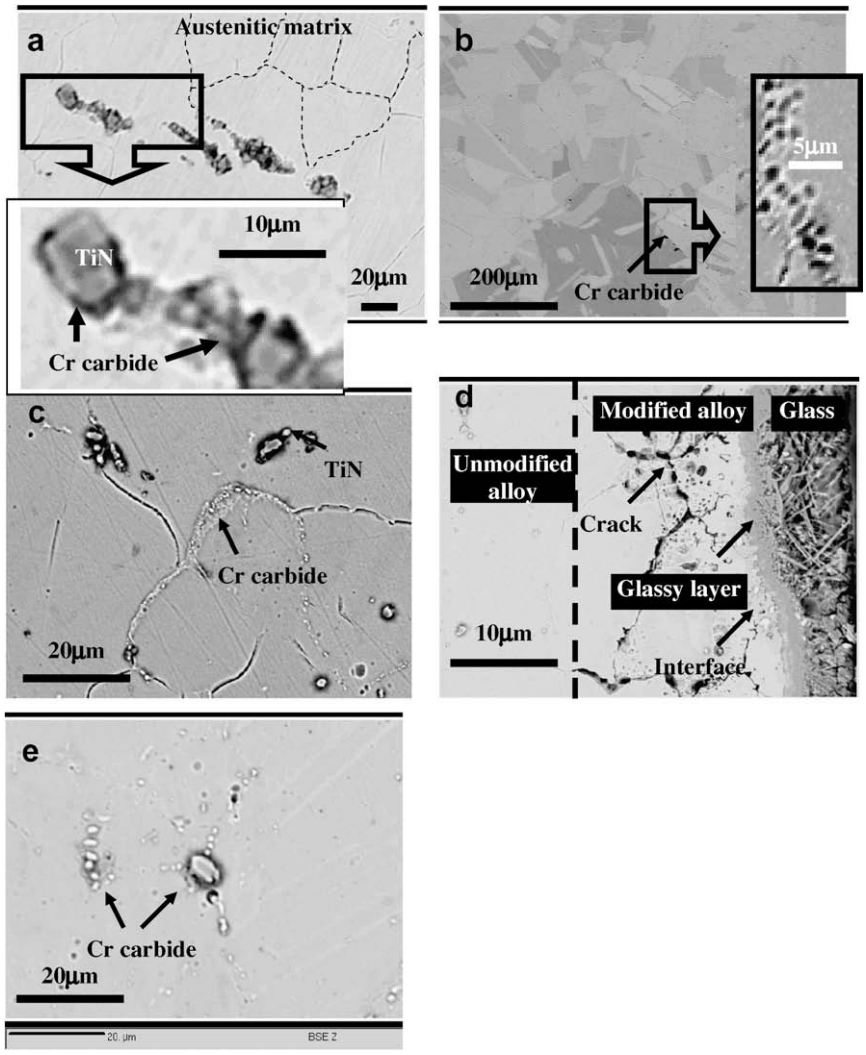

Fig. 2. (a)–(c) BSE images showing the various modes of distribution of TiN and Cr carbide precipitate within the austenitic matrix of as received mill annealed alloy 690. (d) and (e) Images showing the changes in microstructure alloy 690 coupon after being interacted with borosilicate melt for 518.40 ks.

690 components of ceramic melters also [3]. Metallurgical examination of alloy 690 drain valve exposed to borosilicate melt pool at 1423 K for seven years, reported significant microstructural changes including internal void formation, grain coarsening and grain boundary precipitation [3]. Significant wall thinning due to interaction with borosilicate melt has also been reported for alloy 690 insert used in ceramic melter pour spout [4]. Apart from these, one interesting aspect that is common for all sorts of failed melters is that alloy 690 components, which never interacted with borosilicate melt, were always found to be in good conditions. For example, in failed ceramic melters, the top head components, vapor space thermowells, heaters were in good conditions even after prolonged vitrification operation [3]. Similarly, for present induction melters also, no material damage was observed within top dish and upper portion of cell where no interaction with borosilicate melt pool takes place. Based on these observations it is felt that interactions of alloy 690 with borosilicate melt pool might play an important role in process pot failures. Literature survey shows that not much in-depth work has been done on mode of interactions between alloy 690 and borosilicate melt pool. Most of the reported data are based on preliminary metallographic and compositional studies. Hence, in present investigations, detailed study on interaction between alloy 690 with borosilicate melt at soaking/pouring stages has been carried out. Results obtained from this study are given below.

2. Experimental procedure

Compositions of commercial alloy 690 and borosilicate melt used for present experiments are given in Tables 1 and 2, respectively. Detail of the experiments carried out is discussed below under two sub-headings (a) sample preparation and (b) chemical analysis.

2.1. Sample preparation

Borosilicate melt used in the present experiment was prepared by mixing known volume of simulated HLW solution with required amount of glass additive slurry. The mixture was dried under infrared lamp, crushed to fine powder and transferred to a sillimanite crucible. The powder was heated at 973 K for 7.20 ks and further heated at the increment of 50 K and kept for 3.60 ks at each stage, till the glass became pourable. The molten vitreous mass was soaked for 7.20 ks at pour temperature (1223 K) for homogenization.

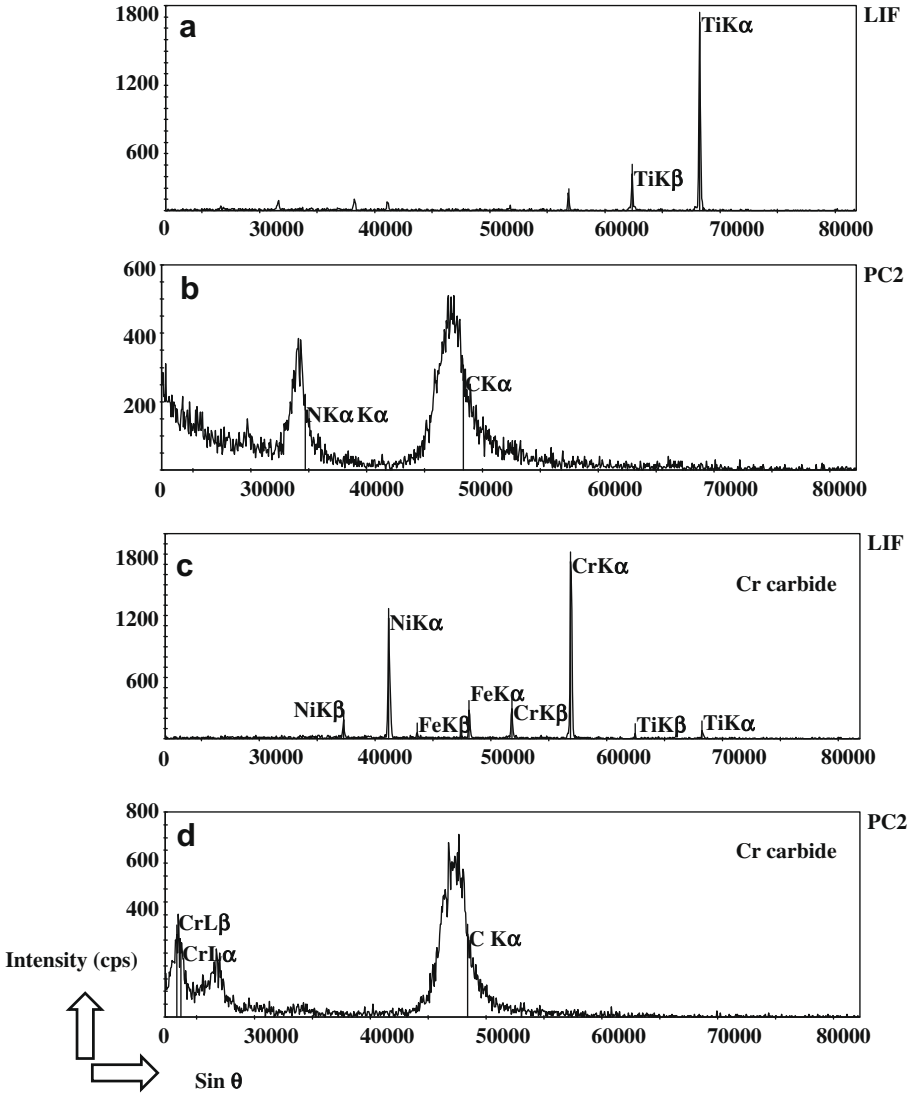

Fig. 3. WDS X-ray spectrums ($\sin\theta \times 10^6$; for better resolution) showing the presence of various elements within TiN (a) and (b) and fine Cr carbides surrounding TiN (c) and (d).

Rectangular coupons of 20 mm × 5 mm × 5 mm dimensions were cut from mill annealed alloy 690 sheet used for fabricating WIP Trombay, process pot. Each of these coupons was drilled on one side, and dipped into borosilicate melt with the help of chromel–alumel wire. The experimental arrangement was done in air atmosphere using a resistance furnace and temperature within borosilicate melt was maintained at 1223 K for different time spans ranging from 28.80 ks to 691.20 ks. In actual plant scale operation, borosilicate melt pool is soaked for ~36.00 ks for homogenization; however, to simulate the effect of repeated cyclic process, experiments were done for longer durations. After each experiment, alloy 690 coupons with adhering borosilicate waste glass were mounted in epoxy resins to grind and polish the cross section of the samples. Polished samples were then analyzed with CAMECA SX 100 Electron Probe Micro-Analyzer (EPMA).

2.2. Chemical analysis

An acceleration voltage of 20 keV and stabilized beam current of 4 nA and 20 nA were used for 'back scattered electron (BSE)' imaging and quantitative analyses respectively. The beam size was kept at ⩽1 μm to reduce the convolution effect so as to arrive at a better estimate of the phase compositions. A program based on Pouchou and Pichoir (PAP) method [5] was used for necessary atomic number (Z), absorption (A) and fluorescence (F) corrections so as to obtain true concentrations from the corresponding raw intensity data.

3. Results and discussion

3.1. Microstructure of as received alloy 690

To simulate actual plant scale situation, no solution annealing heat treatment was given to as received mill annealed specimens. Microstructures of these specimens are shown in Fig. 2(a)–(c). It is observed that alloy 690 is constituted of equiaxed austenitic with varying from 50–80 μm. Isolated intragranular blocky precipitates (2–10 μm) are found to be randomly distributed within the matrix. Enlarged view of these precipitates is shown in inset of Fig. 2(a). Wavelength dispersive spectra obtained from these precipitates identify them as TiN (Fig. 3(a) and (b)). Carbon is also found to be present within these precipitates and hence they are essentially titanium carbonitrates [6]. Surrounding the titanium carbonitrates, fine precipitates are found to occur (Fig. 2(a)). X-ray analysis of these fine precipitates identifies them as Cr carbides (Fig. 3(c) and (d)). Ni, Fe and Ti signals found within X-ray spectra are from TiN and adjacent matrix. Owing to extremely fine size, exact quantitative compositional analysis of Cr carbide precipitates could not be determined. However, earlier Dutta and Tewari identified such carbides as $Cr_{23}C_6$ type [6].In addition to these, discrete Cr carbide precipitates (1–2 μm) are also seen at the grain boundaries (marked in Fig. 2(b) and also shown in inset). These are also considered to be of $Cr_{23}C_6$ type [7]. Further, dense clusters of sub-micron Cr carbide precipitates are noted along certain grain boundaries (Fig. 2(c)), which probably reflect initial growth stage of Cr carbide precipitates after nucleation [7].

3.2. Microstructural changes within alloy 690 coupons after interaction with borosilicate melt

Original microstructures of alloy 690 coupons are found to undergo certain changes upon exposure to borosilicate melt. Fig. 2(d) and (e) shows representative microstructures of the coupon exposed to borosilicate melt for 518.40 ks. It is observed that after the said exposure, coupons suffered from intergranular attack and the initial straight alloy/waste glass interfaces became irregular in nature. Both these microstructures are indicative of material loss

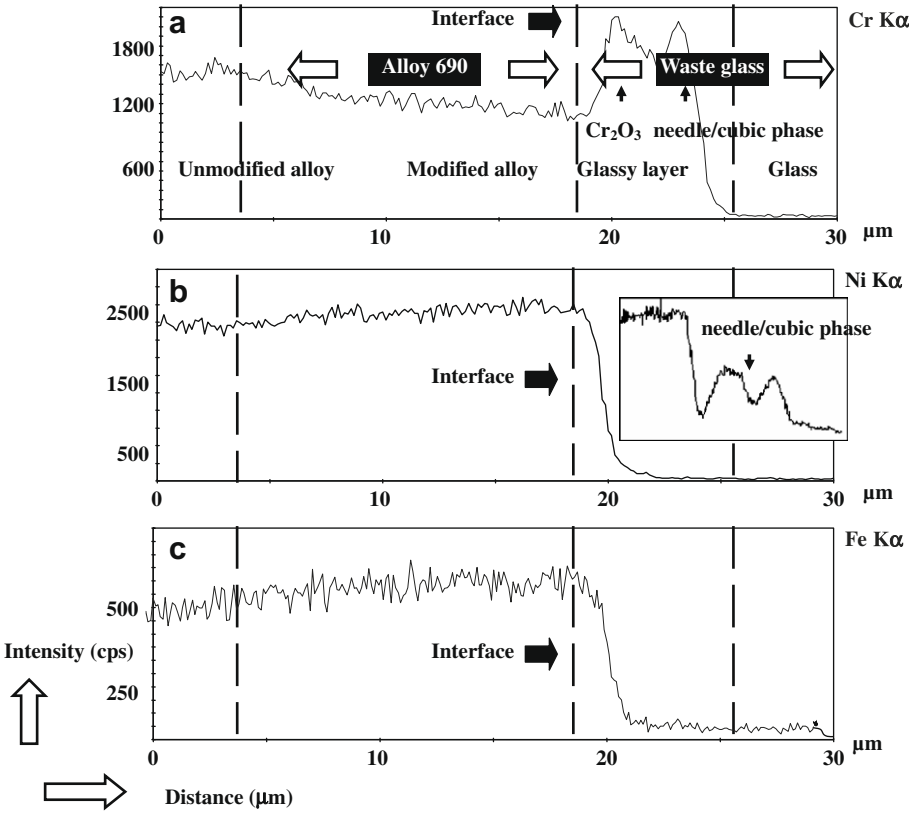

Fig. 4. (a)–(c) X-ray line scans showing distributions of different domains in alloy 690/waste glass couple annealed for 28.80 ks and compositional variations of major components of alloy 690 within these domains. Inset (Ni Kα profile) shows the presence of needle/cubic at the interface for the couple annealed for 518.40 ks.

from the coupons. Elemental line scans taken across the grain boundaries show the presence of waste glass components such as Al, Si etc. This indicates that the borosilicate melt entered within the coupon through grain boundary openings. Apart from these, formations of coarse, discrete, globular Cr carbide precipitates (~5 μm) along grain boundaries and at triple point junctions (Fig. 2(e)) are also observed. Earlier, Kai et al. [8] reported the formation of similar coarse, discrete Cr carbide precipitates along grain boundaries of γ matrix upon prolonged heat treatment at lower temperatures (more than 720.00 ks at ~873 K) or over short duration at higher temperature (3.60 ks at ~1073 K). They also studied the evolution of grain boundary composition with heat treatment schedule using Analytical Electron Microscope (AEM) and found that ~36% Cr depletion (from initial ~28 wt% to 18 wt% after heat treatment) took place at 811 K/3600.00 ks or at 873 K/172.80 ks.

Besides the grain boundary effects, compositional modifications within alloy matrix has also been noted near the interfaces. To establish this, elemental line scans were taken across the alloy 690/waste glass interfaces for all samples and representative profiles obtained from the couple annealed for 28.80 ks are shown in Fig. 4(a)–(c). It is noted that close to interfaces, matrices got depleted in Cr and hence got enriched in Ni and Fe respectively. Similar compositional modifications within alloys 625 and 690 have been reported earlier by Sengupta et al. [9] and Mirschinka et al. [10], respectively. Based on analytical data, two domains namely (i) unmodified and (ii) modified alloy 690 have been delineated for each of the samples. These domains are marked in Fig. 2(d). Among the various elemental scans taken across the couples, Cr Kα profiles are found to be the best ones to delineate the 'modified alloy' widths. This is probably due to higher diffusivity of Cr to borosilicate melt as compared to Fe and Ni. Fig. 5(a)–(c) shows the Cr Kα profiles for three different couples and indicate the general trend of increase in modified alloy widths with time. Table 3 lists the modified alloy domain widths measured from different samples.

In general, the extent of compositional modifications such as this is likely to grow with time following a kinetic relationship of the type,

$$x = kt^{1/n}, \tag{1}$$

where x is reaction layer width, t is time, k is reaction rate constant and n is reaction index. For solid state reactions n assumes a value of 2 and thus the above reaction takes the form of

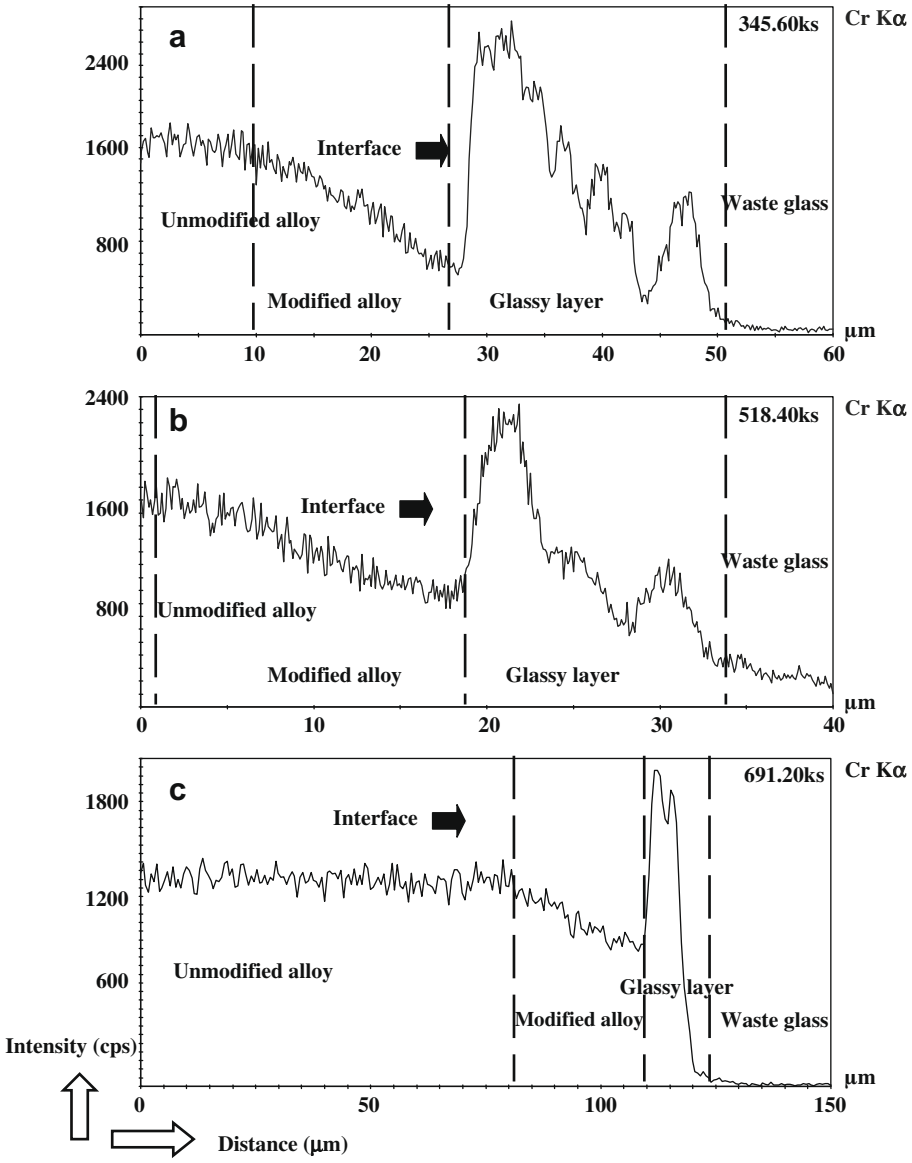

Fig. 5. (a)–(c) Cr Kα X-ray line scans showing distributions of different domains in alloy 690/waste glass couples annealed for different time intervals.

Table 3
Time dependence of modified alloy domains' width

Time (ks)	28.80	172.80	345.60	518.40	691.20
Width (μm)	13	15	16	18	20

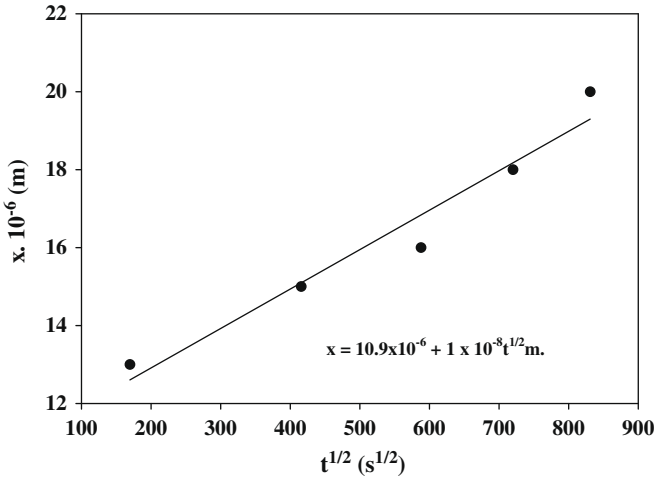

Fig. 6. Time dependence of modified alloy widths.

$$x = kt^{1/2}. \quad (2)$$

To obtain the growth kinetics for present case, widths of the modified alloy domains have been plotted against square root of time (Fig. 6). Fitting of these data with least mean square analysis suggests a kinetic relationship of the type

$$x = 10.9 \times 10^{-6} + 1 \times 10^{-8} t^{1/2}\ \text{m}. \quad (3)$$

Thus, according to this relationship, Cr depleted zone of ~11 μm is likely to form instantaneously within alloy 690 upon its interaction with borosilicate melt. On the other hand, 1000 h exposure of alloy 690 to borosilicate melt will result in ~28 μm wide Cr depleted zone.

Quantitative compositional analyses of alloy 690 matrices close to interfaces have been determined for all the samples and the values are tabulated in Table 4. Decrease of Cr concentration in matrix from initial ~29 wt% to as low as ~14 wt% is noted. This corresponds to a reduction of ~50%, which is quite alarming as Cr offers resistance to intergranular and intergranular stress corrosion cracking attacks in Ni-base alloys [11]. Literature data suggests that the critical Cr concentration required for resisting stress corrosion cracking around grain boundary in Ni–Cr–Fe alloys is ~8–10 wt% [8].

3.3. Microstructural changes within waste glass

EPMA analyses on waste glass adhering to alloy 690 surface, shows interesting physico-chemical changes (Fig. 2(d)). It is observed that within waste glass, three types of phases namely layer, needle and cubic phases have developed close to interface. X-ray line scans taken across the interfaces (Fig. 4(a)–(c)) show two Cr peaks corresponding to Cr_2O_3 and needle/cubic phases, respectively. Ni Kα profile shows a small hump corresponding to needle/cubic phases. It may be added here that X-ray peaks for needle or cubic phases could not be resolved clearly in many cases, due to their fine sizes and close associations. Quantitative analyses of layer, needle and cubic phase identified them as Cr_2O_3, Ni_2CrO_4 and $NiCr_2O_4$ respectively. More detailed account on waste glass microstructure is discussed elsewhere [12]. In an earlier investigation Imrich et al. [4] reported formation of $NiFe_2O_4$ and Cr_2O_3 on alloy 690 insert exposed to borosilicate melt containing ~13 wt% Fe_2O_3 at 1273 K for three months. According to Jantzen et al. [13], under oxidizing conditions Ni rich alloys develop $NiCr_2O_4$ and NiO. This free NiO combines with Fe_2O_3 present within waste glass to form $NiFe_2O_4$. In the present case, Fe_2O_3 content in waste glass is marginal (~6 g/l in HLW) and hence $NiFe_2O_4$ did not form within waste glass. Besides the formation of Ni–Cr rich phases, slight enrichment of Na along the interfaces is also noted in present study. Similar local enrichment in Na concentration at the interface has been reported earlier also [14]. Such local build up in Na concentration is of concern for vitrification of sulfate rich HLW, as it can stabilize water soluble yellow phase at the interface, which can act as sink for radioactive ^{137}Cs and ^{90}Sr. Further, localization of S concentration can influence the nature of intergranular attack within Ni–Cr–Fe alloy [15].

Table 4
Variations in alloy 690 compositions (wt%) near the interface for the sample annealed for different time intervals

Composition	Ni	Cr	Fe	Mn	Al	Si
As received material	60.72	28.79	9.78	0.16	0.12	0.41
172.80 ks	66.74	21.63	10.83	0.00	0.24	0.66
345.60 ks	73.48	15.00	11.02	0.00	0.19	0.33
518.40 ks	75.28	14.11	10.22	0.00	0.05	0.39
691.20 ks	75.51	13.68	10.27	0.06	0.07	0.41

4. Summary

The above experimental results clearly indicate that significant microstructural and compositional variations can take place in alloy 690 process pot and borosilicate melt during plant scale vitrification process. Microstructural changes observed within alloy 690 include (i) discrete Cr carbide precipitation along grain boundaries, (ii) significant depletion of Cr content within austenitic matrix close to interface and (iii) initiation of intergranular attacks at the interface. Each of these aspects can influence the longevity of process pot significantly. Extent of compositional modification of the alloy 690 is found to follow layer growth kinetics of the type $x = 10.9 \times 10^{-6} + 1 \times 10^{-8} t^{1/2}$ m. Despite the fact the extent of compositional modification is small but it may play crucial roles in generation or propagation of factors responsible for process pot failures. Thus compositional modification aspects need to be considered seriously for any efforts towards reduction and/or prevention of process pot failures.

Acknowledgements

The authors are grateful to Dr S. Banerjee, Director, BARC and Mr K. Raj, Head, Waste Management Division, BARC for their keen interest in the work. Mrs Soudamini N. is also acknowledged for experimental help.

References

[1] K. Raj, in: Proceedings Nuclear Fuel Cycle Technologies: Closing The Fuel Cycle, Kalpakkam, 2003, p. 1.
[2] C.P. Kaushik, R.K. Mishra, P. Sengupta, Amar Kumar, D. Das, G.B. Kale, K. Raj, J. Nucl. Mater. 358 (2006) 129.
[3] D.C. Iverson, K.J. Imrich, D.F. Bickford, J.T. Gee, C.F. Jenkins, F.M. Heckendorn, Ceram. Trans. 155 (2004) 217.
[4] K.J. Imrich, D.C. Iverson, Ceram. Trans. 107 (2000) 643.
[5] J.L. Poucho, F. Pichoir, Microbeam Analysis, San Francisco, 1988, p. 319.
[6] R.S. Dutta, R. Tewari, Brit. Corros. J. 34 (1999) 201.
[7] Y.S. Lim, J.S. Kim, H.P. Kim, H.D. Cho, J. Nucl. Mater. 335 (2004) 108.
[8] J.J. Kai, G.P. Yu, C.H. TSAI, M.N. Liu, S.C. Yao, Metall. Trans. A 20A (1989) 2057.

[9] P. Sengupta, J. Mitra, G.B. Kale, J. Nucl. Mater. 350 (2006) 66.
[10] V. Mirschinka, S. Halazovich, R. Odoj, Mater. Res. Soc. Symp. Proc. 15 (1983) 695.
[11] H. Sahlaoui, H. Sidhom, J. Philbert, Acta Mater. 50 (2002) 1383.
[12] P. Sengupta, C.P. Kaushik, R.K. Mishra, G.B. Kale, J. Am. Ceram. Soc. (in press).
[13] C.M. Jantzen, A.D. Cozzi, N.E. Bibler, Ceram. Trans. (168) 31.
[14] V. Kain, P. Sengupta, P.K. De, S. Banerjee, Metall. Trans. A 36A (2005) 1075.
[15] R. Bandy, R. Roberge, R.C. Newman, Corros. Sci. 23 (1983) 995.